Rotating flow instability prediction using eigenvalue analysis

Shenren Xu *[1]
[1]*School of Power and Energy, Northwestern Polytechnical University, Xi'an, 710072, China*

The compression system in turbomachines, e.g., aircraft engines and gas turbines, when operating under off-design conditions, exhibits self-excited unsteady phenomena such as surge, rotating stall and rotating instability, leading to performance deterioration and/or structural damages. Inability to accurately predict when such flow instability occurs limits the development of high performance compression system. In this paper, an eigenvalue problem is solver to (1) predict the linear stability and (2) find the destabilizing eigenmode for a classical commonly seen for turbomachines operating at near stall conditions. The eigenvalue analysis is fully based on the steady state three-dimensional Reynods-averaged Navier-Stokes equations and thus the stability boundary is fully consistent with the one that is predicted by the time-accurate flow simulation, i.e., URANS, but two to three times faster. The method is applied to the computation of stability boundary of (i) the laminar flow around a two-dimensional circular cylinder, (ii) the flow around a quasi-three-dimensional compressor anuular cascade, and (iii) flow around a three-dimensional compressor rotor. The method developed here has the potential to revive the once-popular eigenvalue method for prediction rotating stall and surge, which was based on lower-fidelity flow models and provide industry with tools to accurately predict the stall line in the early design stage.

I. Todo list

- Investigate the fouriour spectrum of the circumferential signal of the eigenvectors and interpret the various frequency components.
- Investigate the influence of the axial location where the circumferential signal is taken.
- Label relevant eigenmodes with NDs.
- Compare unstable modes with URANS.

II. Introduction

Rotating stall and rotating instability has been studied extensively both experimentally and numerically. However, previous numerical investigations mainly focused on using time-dependent unsteady flow analysis using a fraction of the

*Corresponding author, email address: shenren_xu@nwpu.edu.cn

annulus. Flow physics for the destablization mechanism has been investigated in depth but little insight has been gained. Eigenvalue analysis is a powerful yet inexpensive tool to probe the flow near the critical condition, revealing rich flow physics with cost comparable to a steady state analysis. In this work, we demonstrate that using eigenvalue analysis based on a whole-annulus steady state solution, the linear stablity demarcation point can be pinpointed with the cost of a few steady state analysis, and a full-annulus time-accurate unsteady calculation can thus be avoid. This methodology enables a quick parameter study to investigate the various rotating flow instability phenomenon such as rotating stall and rotating instability.

III. The nonlinear flow solver

A. Governing equations

B. Spatial discretization

C. Temporal discretization

IV. Global linear stability analysis

For a nonlinear dynamic system, e.g., the discretised NS equation, using the method of lines, the governing equation is

$$\frac{d\mathbf{u}}{dt} = -\mathbf{R}(\mathbf{u}) \tag{1}$$

where $\mathbf{u}$ is the time-varying flow variable and $\mathbf{R}(\mathbf{u})$ is the nonlinear residual representating the spatial discretization. Assuming a steady state solution $\mathbf{u}_0$ (equilibrium point of the dynamic system) exists, and the time-varying flwo variable can be decomposed as the steady and the unsteady part

$$\mathbf{u} := \mathbf{u}_0 + \tilde{\mathbf{u}} \tag{2}$$

and the governing equation becomes

$$\frac{d\tilde{\mathbf{u}}}{dt} = A\tilde{\mathbf{u}} \tag{3}$$

where A is the negative Jacobian $A := -\dfrac{\partial \mathbf{R}}{\partial \mathbf{u}}$.

In order to use the eigen model decomposition approach, suppose the system matrix has right eigenvectors $\{\mathbf{v}_i, \mathbf{v}_2, ..., \mathbf{v}_N\}$, which forms the matrix V as its colum vectors. Matrix A can then be factorized as

$$A = V\Lambda V^{-1} \tag{4}$$

where the diagonal matrix Λ has the eigenvalues on the matrix A as its diagonal elements. Decomposing the unsteady

part $\tilde{\mathbf{u}}$ in the eigen modal space, it can be expressed as a linear combination of all eigenvectors with coordinates η

$$\tilde{\mathbf{u}} = V\eta \tag{5}$$

Substituting the $\tilde{\mathbf{u}}$ in the governing equation using the eigen modal decomposition, it becomes

$$\frac{d\eta}{dt} = \Lambda\eta \tag{6}$$

Different from the original coupled system, all variables are decoupled now and it can be written as

$$\frac{d\eta_i}{dt} = \lambda_i\eta_i \quad \forall i \tag{7}$$

For the linear system to be stable, the sufficient and necessary condition is that all eigenvalues has a negative real part, i.e., $\text{real}(\lambda_i), \forall i$.

A. Numerical implementation

In practice, performing the global linear stability analysis as described above is a standard procedure involving three steps:

- Find an equilirium point (converging to steady state solution);
- Linearize the nonlinear residual and form the Jacobian matrix;
- Calculate the eigenvalue with the largest real part.

B. Time-domain unsteady approach

C. Eigenvalue approach

V. Eigenvalue analysis for large sparse matrices

VI. Results

A. Laminar flow around a two-dimensional circular cylinder

Eigenvalue analysis is performed for the canonical case of the laminar flow around a circular cylinder with the Reynolds number in the range between 40 and 100. The computational domain is a circular cylinder centered at the origin with a diameter of $D = 10^{-5}$ and the farfield is a circle with a diameter of $100D$. The left half of the outer circle is set to 'farfield' boundary condition with a incoming flow of Mach 0.2 in the x-direction, a static pressure of 101325 Pa and and a temperature of 288.15 K. The right half ot he circle is set to 'pressure-outlet' boundary condition, with a constant pressure of 101325 Pa. The computational domain is meshed with quadrilateral elements, with a total

of 29600 grid points. The density is 1.225 kg/m^3. The dynamic viscosity is varied in order to achieve a particular Reynolds number.

1. Steady state calculation

The steady state flow is obtained by either using an implicit solution method in Fluent (version 19.2) or by resorting to the Newton-Krylov algorithm in NutsCFD, despite the fact that the flow is physically unsteady under this condition. The Mach number contour of the NutsCFD calculation is shown in Fig. 1.

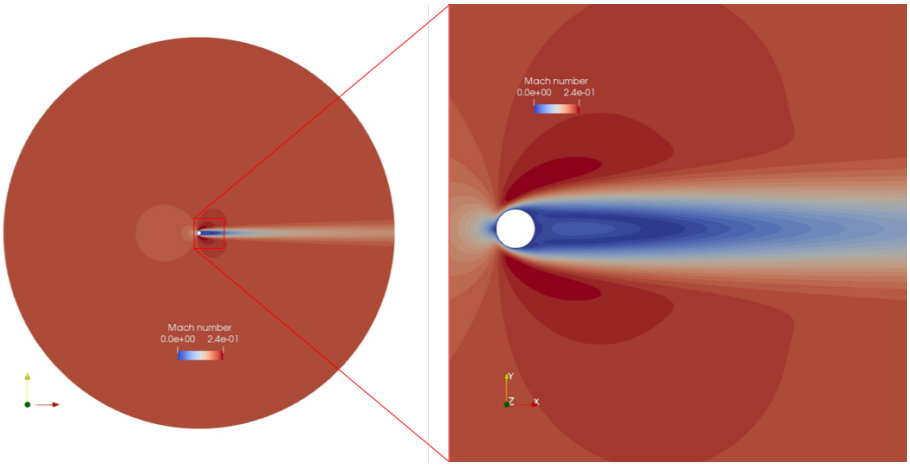

Fig. 1 Mach number contour plot of the calculation results by NutsCFD for Re = 55.

To compare the Fluent and NutsCFD results quantitatively, the velocity-x behind the cylinder as well as the pressure coefficient along the cylinder surface are compared in Fig. 2 and very good agreement can be found.

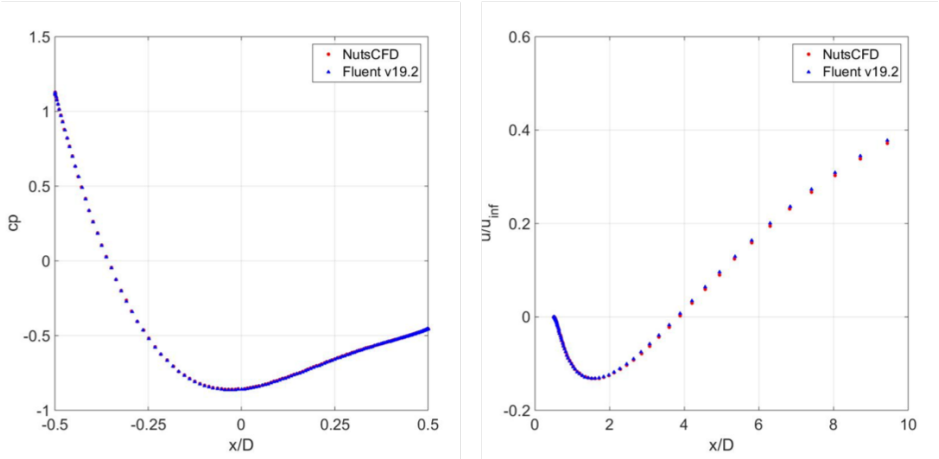

Fig. 2 Comparison between Fluent and NutsCFD calculation results for velocity-x along the center line behind the cylinder (left) and pressure coefficient along the cylinder surface (right).

2. Unsteady calculation

Experimental results show that the laminar flow around the cylinder becomes unsteady for Re above a critical value (around 47). To study this phenomenon, unsteady flow calculation for $Re = 55$ and $Re = 40$ are performed using Fluent. First, for both conditions, a steady state flow solution is obtained by converged the residual to machine error. For $Re = 55$, the unsteady simulation is run with the steady state as initial condition. A BDF2 second-order implicit dual-time-stepping method is used with the physical time step set to $10^{-8} sec$, that is, $0.01 ms$, and the inner loop is solved with a CFL of 1000 and maximum 5 iterations. Roughly two orders of magnitude of residual drop is achieved for the inner loop. From Fig. 3, it can be seen that after around $100 ms$, the lift coefficient starts to grow and eventually reaches a saturated limit cycle at around $130 ms$. On the contrary, running unsteady simulation with a fully converged steady state for $Re = 40$ does not lead to unsteadiness. To probe the flow at $Re = 40$ further, a disturbance is introduced into the flow from the farfield by setting the incoming flow direction to vertical for one time step and switching it back to the horizontal direction, and then continue the unsteady run. The lift coefficient shows a transient response but eventually slowly delays to zero. These two sets of lift coefficient signals are plotted in Fig. 3 in both linear and logrithm scales. The logrithmic plot on the right clearly shows an exponential growth and decay for $Re = 55$ and $Re = 40$, respectively.

The growth and decay rate for both conditions can be extracted from the time signal and then be compared to the eigenvalue analysis results.

The same unsteady simulation is not performed in NutsCFD as the code is slower than fluent and in the meantime, it is believed that the unsteady response between the two solvers will be very similar, based on the comparison of the steady state solutions.

3. Eigenvalue analysis

An eigenvalue analysis is performed for the steady state solution calculated in NutsCFD. After converging the steady state solver to machine error ($tol = 10^{-14}$), the exact Jacobian matrix based on the 2nd-order spatial accuracy is calculated and output to file. The sparse matrix is read into Matlab and eigs is used to compute a subset of the eigenvalues, with the aim of finding the (hopefully one) unstable mode. To minimize the computational effort, 10 eigenvalues/vectors are computed for matrices with different shifts of $0, i, 2i, 3i, 4i, 5i$. All the eigenvalues, 60 in total and with some duplicated, are plotted in Fig. 4. It can be seen that there is one eigenvalue that is on the right side of the imaginary axis, indicating there is one unstable mode. In the meantime, from the time-domain simulation, one can extract from the lift-coefficient signal that the flow is linearly growing with a growth rate of 0.123 and oscillating with a circular frequency of $4.94 rad/s$. This mode is plotted along with the spectrum and it can be seen that this mode also overlaps with the unstable eigenvalue from the eigenanalysis.

The eigenanalysis not only generates the eigenvalues but also the eigenvectors associated with each eigenvalue. For the unstable mode, the real part of the density, x/y momentum and energy component of the unstable eigenvector is

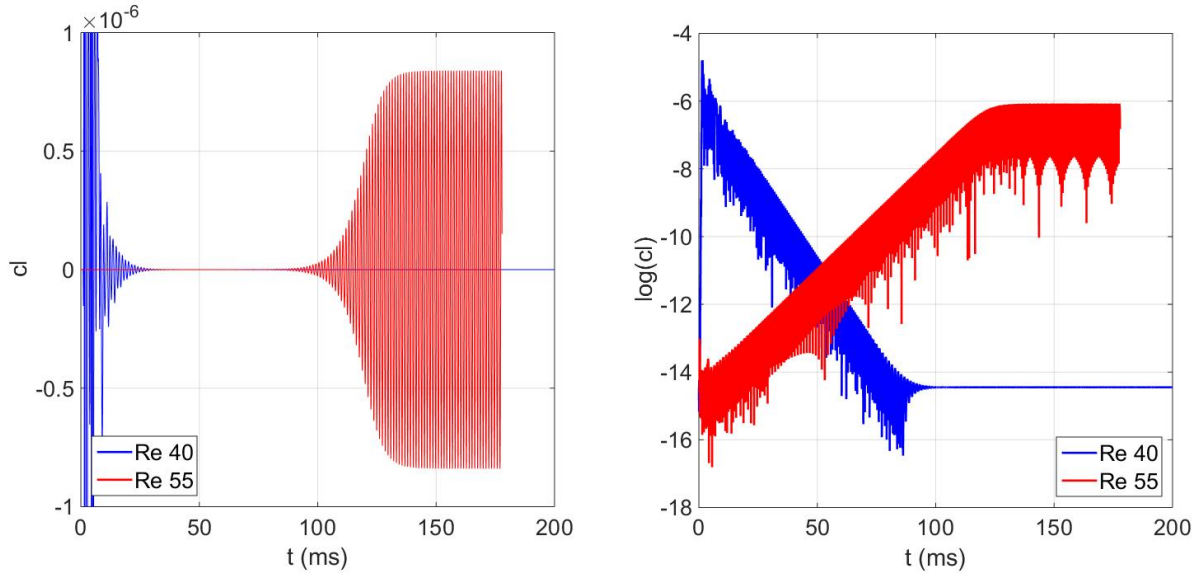

Fig. 3 Lift coeffient histogram for $Re = 55$ and $Re = 40$.

shown in Fig.5.

B. Transonic flow for a single blade (quasi-3D analysis)

NutsCFD is used to analyze the performance of the first stage rotor (NASA Rotor 67) of a two stage transonic fan designed and tested at the NASA Glenn center [1]. Its design pressure ratio is 1.63, at a mass flow rate of 33.25 kg/sec. The NASA Rotor 67 has 22 blades with tip radii of 25.7 cm and 24.25 cm at the leading and trailing edge, respectively, and a constant tip clearance of 1.0 mm. The hub to tip radius ratio is 0.375 at the leading edge (TC = 0.6% span) and 0.478 at the trailing edge (TC = 0.75% span). The design rotational speed is 16,043 RPM, and the tip leading edge speed is 429 m/s with a tip relative Mach number of 1.38.

C. Compressor performance characteristics

Steady state analysis is performed for both the single-passage and whole-annulus configurations. In order to obtain the steady state solutions for the whole annulus, which presumably is identical for each blade passage, we first compute the steady state solution for one passage with rotatioal periodicity, and then copy the solution to the whoe annulus using rotational transformation. The pressure ratio and efficiency are shown in Fig. 6 which is produced by incrementally raising the back pressure from the inlet total condition. It can be seen that there is small difference (mainly efficiency) between the single-passae and whole-annulus results, which is due to the minor discrepancy of the spatial discretization at the periodic boundaries for single passage calculation.

The flow solution using either single passage or whole annulus is shown in Fig. 7, which visually shows that the

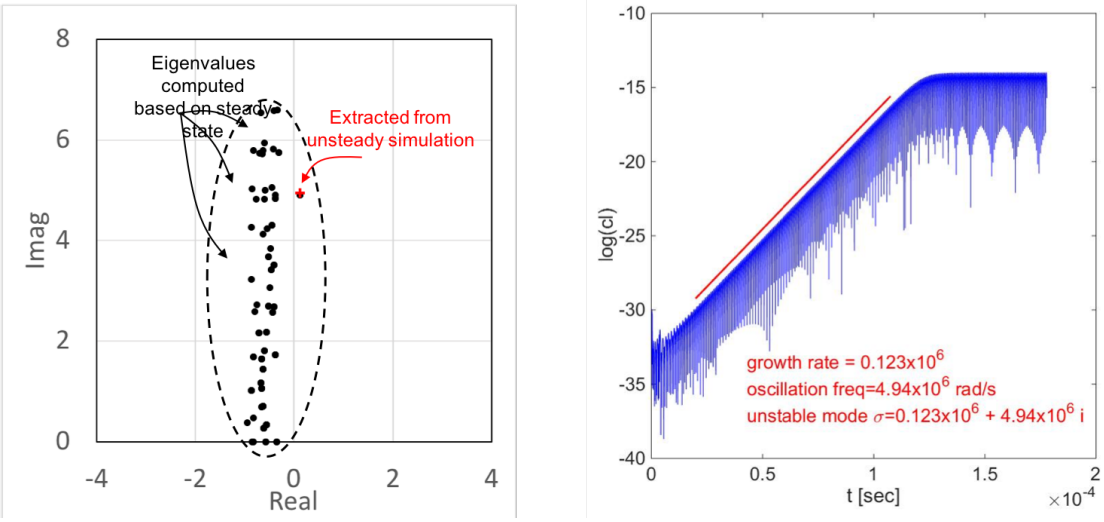

Fig. 4 Eigenspectrum from the steady state eigenvalue analysis compared with the linearly destabiling unsteady simulation for $Re = 55$.

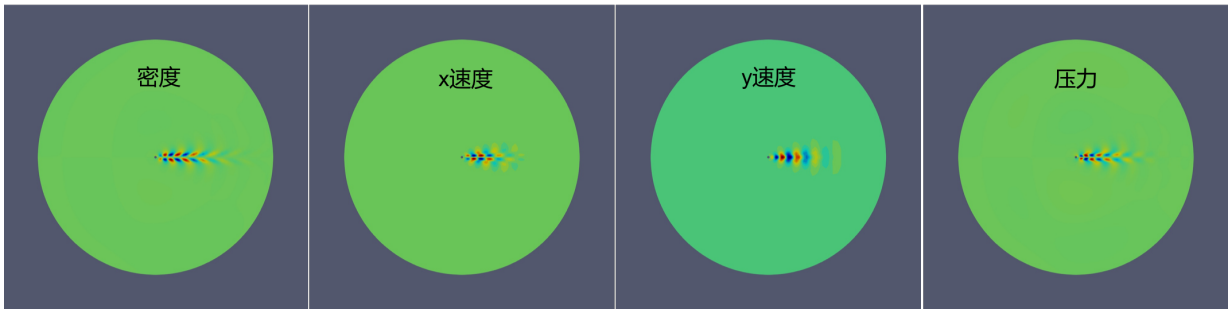

Fig. 5 Real part of the density, x/y momentum, energy components of the unstable eigenmode for $Re = 55$.

solutions are not distinguishable.

D. Eigenvalue analysis

For each whole-annulus steady state solution, an eigenvalue analysis is performed using the Jacobian matrix output from the NutsCFD solver once the steady state calculation has fully converged. Since the rotational speed for the rotor is 16,043 RPM, the Jacobian matrix is scaled by a factor of $1/(2\pi \times 16,043/60) \approx 1/1680$, so that all frequencies involved in this computation is reduced by the rotor angular frequency. This is done due to the pre-knowledge that rotating stall cells move with speed of the same order of magnitude.

Shown in Fig. 8 is a subset of the eigenvalues that are near the imaginary axis, which presumally are most likely to be unstable. The eigs function in Matlab is used with various imaginery shifts to compute interior eigenvalues. The ones that are suspecious of crossing the imaginery axis are shown. A zoomed view of the eigenvalues reveals that there are a total of five that have positive real parts, i.e., unstable. The pressure component of the eigenvector corresponding to the 3rd eigenvalue is visualized to the right of Fig. 8. The circumferential synchronized shock oscillation can be

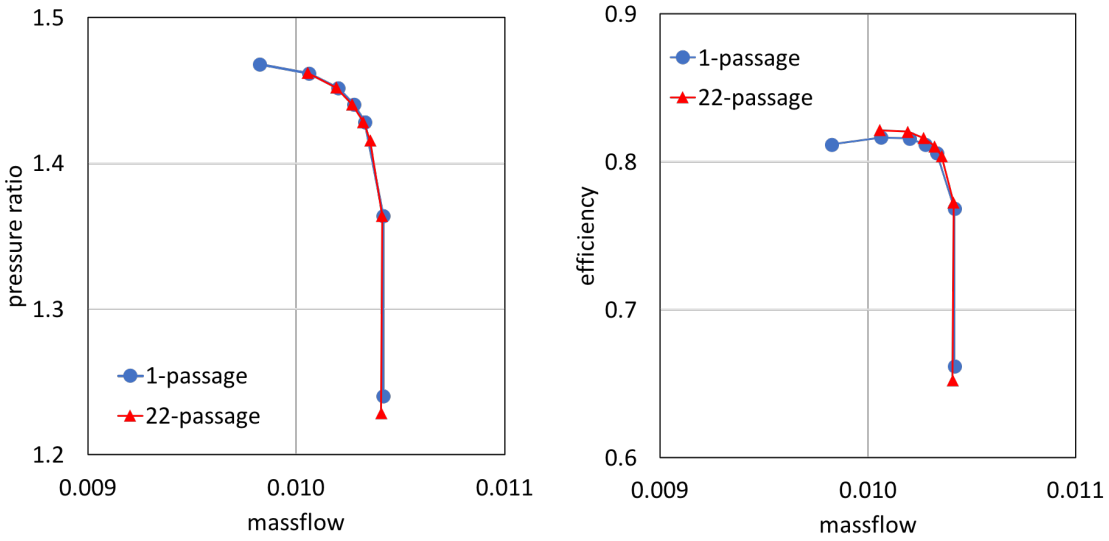

Fig. 6 Q3D performance for rotor67 at 50% blade height with either single passage or whole annulus (22 passages).

easily spotted. Eigenvectors of other unstable mode are similar, except with different circumferential variation, which can further be attributed to different nodal diameters, which varies from 5 to 9, continuously, from eigenvalues 1 to 5.

Nodal diamater for different eigenmodes?

VII. Conclusion

Acknowledgements

References

[1] Strazisar, A. J., Wood, J. R., Hathaway, M. D., and Suder, K. L., "Laser anemometer measurements in a transonic axial-flow fan rotor," 1989.

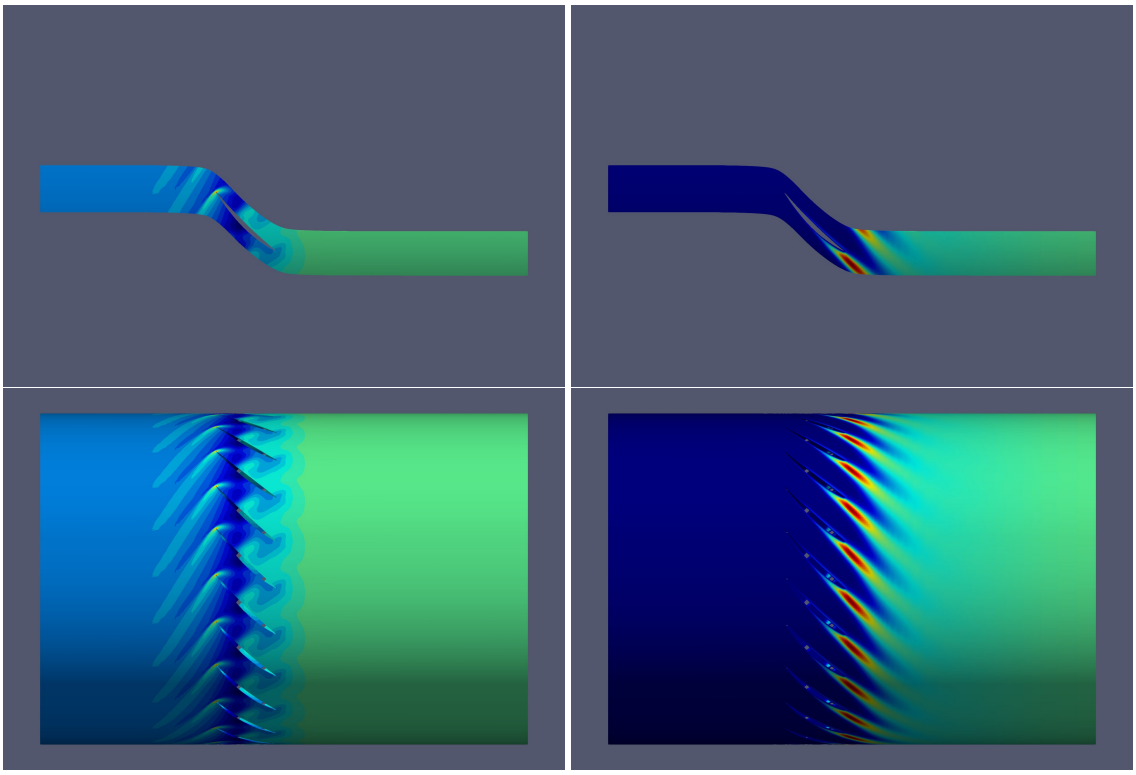

Fig. 7 Pressure (left) and SA variable (right) contours for single passage (top) and whole annulus (bottom) calculations.

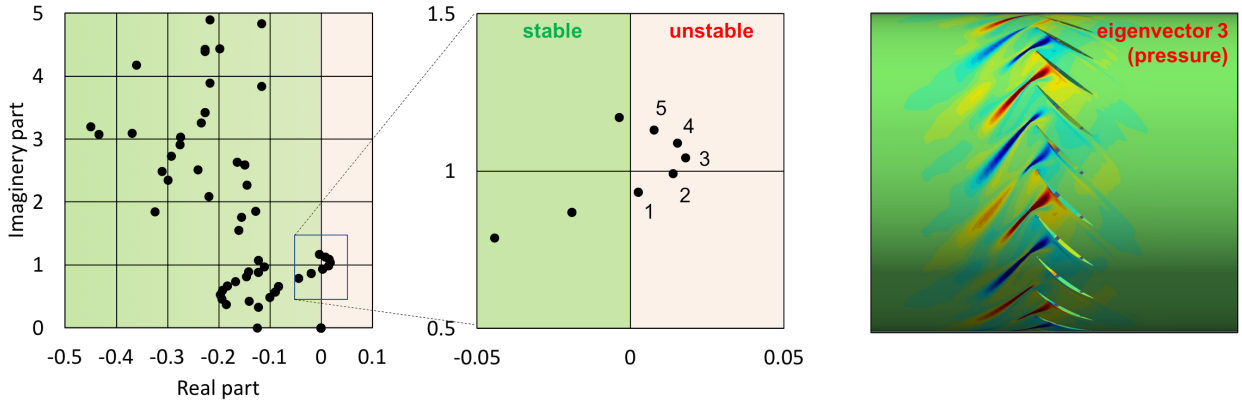

Fig. 8 18kpa eigenvalue.

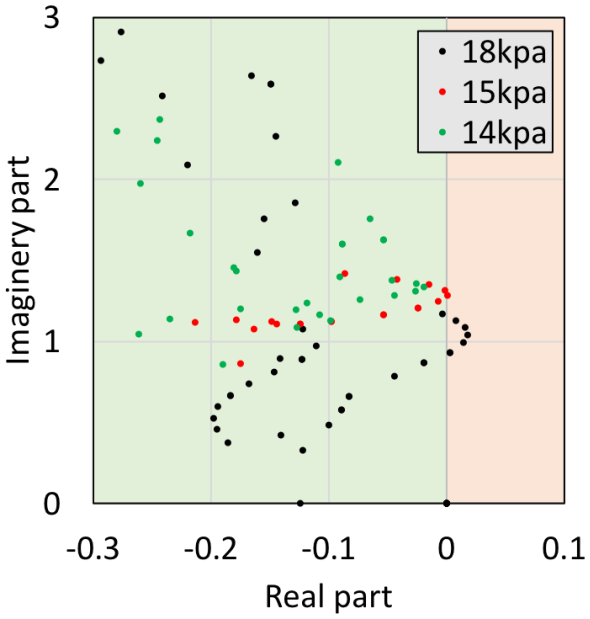

Fig. 9 18kpa eigenvalue.